P122 | Advanced Topics in Plasma Physics

Hydrodynamic and Magnetohydrodynamic Turbulence

Instructor: Muni Zhou

These notes build a physical picture of turbulent energy transfer, from hydrodynamic eddies to magnetized fluctuations. The first part develops the Kolmogorov and GS95 cascades using amplitudes, lengths, and competing times. The second introduces the MHD energy and helicity conservation laws. Magnetic helicity leads to flux linkage and Taylor relaxation; cross helicity then leads to Alfvénic relaxation and the Elsasser description of interacting wave packets.
The relation between cross helicity and Elsasser energies introduces imbalanced turbulence. Dynamic alignment and intermittency then connect the geometry and statistics of fluctuations to the cascade. Each derivation keeps the essential physical steps and identifies the additional assumptions needed for a scaling model.

Dartmouth College

Graduate plasma physics

Contents

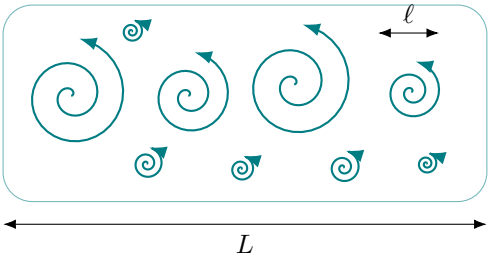
1 The language of scales **1**
1.1 Eddies, fluctuations, and relative motion . . . 1
1.2 What a cascade theory predicts . . . 1
2 Hydrodynamic dynamics and energy transfer **2**
2.1 The equations and the energy budget . . . 2
2.2 How a nonlinear term creates shorter scales . . . 2
2.3 A physical picture of the cascade . . . 3
3 The Kolmogorov cascade **3**
3.1 Two assumptions and one transfer time . . . 3
3.2 From an amplitude to the spectrum . . . 4
3.3 The cutoff, the cascade time, and locality . . . 4
4 What the magnetic field adds **5**
4.1 The MHD equations and the magnetic force . . . 5
4.2 Stretching and flux freezing . . . 6
4.3 Alfvén waves and anisotropy . . . 6
5 Weak and strong turbulence **7**
5.1 Two times and the strength of an encounter . . . 7
5.2 The weak-cascade baseline . . . 7
6 Critical balance and the GS95 cascade **8**
6.1 Critical balance as a physical hypothesis . . . 8
6.2 Amplitude, spectrum, and anisotropy . . . 9
6.3 How far can this model be continued? . . . 10
7 Quadratic invariants and selective decay **11**
7.1 Magnetic helicity: definition and gauge invariance . . . 12
7.2 What can survive while energy decays? . . . 12
8 Magnetic helicity: flux linkage and Taylor relaxation **13**
8.1 Magnetic flux and the meaning of helicity . . . 13
8.2 Two linked flux tubes . . . 13
8.3 Twist and reconnection . . . 14
8.4 Minimum magnetic energy at fixed helicity . . . 15
8.5 Finding a relaxed field in a given domain . . . 16
9 Cross helicity and Alfvénic relaxation **17**
9.1 Cross helicity and the energy bound . . . 17
9.2 Selective decay toward an Alfvénic state . . . 17
10 Elsasser variables, wave packets, and imbalance **17**
10.1 Definitions and inverse relations . . . 17
10.2 Energy and cross helicity in Elsasser variables . . . 18
10.3 Adding and subtracting the equations . . . 18
10.4 Fluctuations about a uniform guide field . . . 19
10.5 Why the opposite population matters . . . 19
10.6 Cross helicity measures population imbalance . . . 20
10.7 Imbalance separates the straining times . . . 20
10.8 Global relaxation and local alignment answer different questions . . . 21
11 Dynamic alignment and three-dimensional structure **21**
11.1 A finite energy flux needs a finite interaction . . . 21
11.2 Three lengths instead of two . . . 21
11.3 An alignment closure and its consequences . . . 22
12 Intermittency **23**
References **25**

1 The language of scales

1.1 Eddies, fluctuations, and relative motion

We use $\boldsymbol{U}$ and $\boldsymbol{B}$ for the physical velocity and magnetic field. Their mean and fluctuating parts are $\boldsymbol{U} = \boldsymbol{U}_0 + \delta\boldsymbol{U}$ and $\boldsymbol{B} = \boldsymbol{B}_0 + \delta\boldsymbol{B}$. Sections 1–6 use the physical magnetic field. From section 7 onward, we express it in velocity units and normalize the vector potential, flux, energy, and helicities consistently.

Turbulence contains irregular motion over a range of sizes. An *eddy* is a correlated region of this motion, characterized by a length ℓ, a velocity difference δU_ℓ, and a lifetime. It need not have a circular outline or a clearly identifiable boundary. Large and small fluctuations coexist in the same fluid.



Large and small fluctuations coexist.

An eddy is a correlated region, characterized by a scale ℓ and a velocity difference δU_ℓ.

Figure 1: Correlated fluctuations coexist across scales. The vortices are schematic symbols for motion, not rigid objects or uniquely bounded eddies.

To describe a fluctuation at scale ℓ, compare velocities at two points separated by that distance:

$$\delta\boldsymbol{U}_\ell(\boldsymbol{x}) = \boldsymbol{U}(\boldsymbol{x}+\boldsymbol{\ell}) - \boldsymbol{U}(\boldsymbol{x}), \qquad \delta U_\ell = \left\langle |\delta\boldsymbol{U}_\ell|^2 \right\rangle^{1/2}. \tag{1.1}$$

Magnetic increments $\delta\boldsymbol{B}_\ell$ and their rms amplitudes δB_ℓ are defined analogously. The scale subscript distinguishes an increment across ℓ from the mean-subtracted fluctuation $\delta\boldsymbol{U} = \boldsymbol{U} - \boldsymbol{U}_0$. A uniform velocity carries the two points together. Their velocity difference describes relative motion and gives an estimate of how quickly a structure changes shape. This is why $\ell/\delta U_\ell$, rather than length divided by the bulk flow speed, enters a cascade model. If the mean flow has appreciable shear, its contribution to the velocity difference must be distinguished from the turbulent fluctuation.

1.2 What a cascade theory predicts

Energy is supplied near an outer scale L, transferred between scales by nonlinear interactions, and ultimately converted to heat or to other forms of particle energy. A cascade theory connects the amplitude, shape, and lifetime of fluctuations along this route. The source can be mechanical stirring, shear, an instability, or astrophysical driving; the questions about transfer are similar.

We use $k \sim \ell^{-1}$ for scale estimates and omit numerical factors such as 2π. Angle brackets denote a volume or statistical average, specified by the problem. Cascade estimates and spectra use energy per unit mass. From section 7 onward, the invariant and relaxation calculations use the normalized volume integrals defined there. After subtracting a uniform mean flow, we write the kinetic-energy spectrum as

$$\frac{1}{2}\left\langle |\delta\boldsymbol{U}|^2 \right\rangle = \int_0^\infty E_U(k)\,\mathrm{d}k. \tag{1.2}$$

Thus $E_U(k)\,\mathrm{d}k$ is energy in a wavenumber interval and $kE_U(k)$ is energy per logarithmic interval. The latter will give a short route from a fluctuation amplitude to a spectrum.

Quantity	Meaning
L, $U_L = \delta U_L$	Outer scale and its characteristic velocity difference
ε	Energy transfer rate per unit mass, with units L^2/T^3
ν, η	Kinematic viscosity and magnetic diffusivity, both with units L^2/T
$\mathrm{Re} = U_L L/\nu$, $\mathrm{Rm} = U_L L/\eta$	Fluid and magnetic Reynolds numbers
$\mathrm{Pm} = \nu/\eta$	Magnetic Prandtl number
$\boldsymbol{U}$, $\boldsymbol{B}$	Velocity and magnetic field; $\boldsymbol{B}$ uses velocity units from section 7
$\ell_\perp$, $\ell_\parallel$	Lengths perpendicular and parallel to the relevant magnetic field
τ_{nl}, τ_{A}, τ_{cas}	Nonlinear distortion, Alfvén propagation, and energy-transfer times

The working questions

What carries the energy? Which process changes a fluctuation? How long does that process take, and what sets the fluctuation's geometry? Start with these questions before choosing a spectral index.

2 Hydrodynamic dynamics and energy transfer

2.1 The equations and the energy budget

For a constant-density, incompressible fluid,

$$\partial_t \boldsymbol{U} + \boldsymbol{U}\cdot\boldsymbol{\nabla}\boldsymbol{U} = -\frac{\boldsymbol{\nabla} p}{\rho_0} + \nu\nabla^2\boldsymbol{U} + \boldsymbol{f}, \qquad \boldsymbol{\nabla}\cdot\boldsymbol{U} = 0. \tag{2.1}$$

Pressure enforces incompressibility, $\boldsymbol{f}$ supplies energy, and viscosity removes kinetic energy. The ratio of nonlinear to viscous acceleration at the outer scale is $\mathrm{Re} = U_L L/\nu$. Large Re allows nonlinear distortion to create gradients before viscosity smooths them.

For a periodic volume, the energy balance is

$$\frac{\mathrm{d}}{\mathrm{d}t}\frac{1}{2}\left\langle U^2\right\rangle = \langle \boldsymbol{U}\cdot\boldsymbol{f}\rangle - \nu\left\langle |\boldsymbol{\nabla}\boldsymbol{U}|^2\right\rangle. \tag{2.2}$$

Nonlinearity redistributes energy while conserving the volume total. In a statistically steady state, mean input equals mean dissipation. A large-scale flow can therefore supply energy that is dissipated only after much smaller gradients have formed.

2.2 How a nonlinear term creates shorter scales

A short scalar example exposes the multiplication of fields in an advective term. Take

$$\partial_t U + U\partial_x U = 0, \qquad U(x,0) = U_L \sin(k_0 x). \tag{2.3}$$

At the initial instant,

$$U\partial_x U = \frac{U_L^2 k_0}{2}\sin(2k_0 x), \qquad U(x,t) \simeq U_L\sin(k_0 x) - \frac{U_L^2 k_0 t}{2}\sin(2k_0 x). \tag{2.4}$$

The nonlinear term immediately produces a shorter wavelength. Repeated interactions can generate further scales. This is a one-dimensional illustration of harmonic generation; three-dimensional incompressible turbulence involves interacting vector fields and pressure as well.

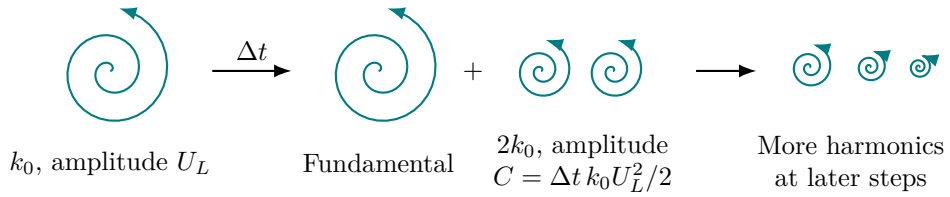


Figure 2: Nonlinear advection generates a shorter wavelength. The first harmonic has the phase in equation (2.4); the circles illustrate wavelength, not a fixed eddy-splitting rule.

2.3 A physical picture of the cascade

A large fluctuation strains and deforms the flow, producing smaller structures. Those structures deform on their own times and create still smaller ones. Energy can move between scales even though all these structures occupy the fluid simultaneously. The cascade is a statistical picture, not a rule that each eddy divides into a fixed number of smaller vortices.

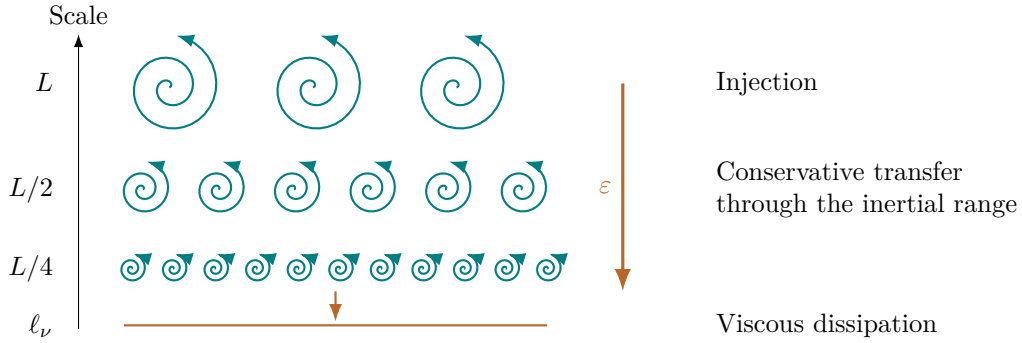


Figure 3: Energy passes through a hierarchy of scales. Each row denotes a scale range; all scales can coexist in the same region of fluid.

The mean flux through an inertial-range scale is the rate at which energy passes from larger to smaller scales. Individual events can transfer energy in either direction; the forward cascade refers to the net flux. This flux need not equal the energy stored at a scale.

Nonlinearity supplies gradients; dissipation acts on them

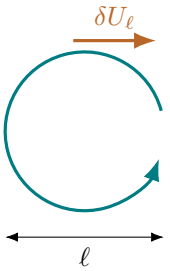
The factor ν in the energy sink can be small while $\langle|\boldsymbol{\nabla U}|^2\rangle$ is large. Thus the dissipation rate can remain finite as Re increases. This observation motivates a cascade whose inertial-range transfer is largely independent of the microscopic viscosity.

3 The Kolmogorov cascade

3.1 Two assumptions and one transfer time

The K41 picture assumes that small inertial-range fluctuations become approximately independent of the details of large-scale forcing, and that their statistics are set by the scale ℓ and a common mean energy flux ε [1, 2]. Local isotropy is part of this baseline picture. The phenomenological transfer time is the time for a velocity difference to deform a structure by its own size:

$$\tau_{\mathrm{nl}}(\ell) \sim \frac{\ell}{\delta U_\ell}, \qquad \tau_{\mathrm{cas}} \sim \tau_{\mathrm{nl}}. \tag{3.1}$$



Nonlinear distortion time:

$$\tau_{\rm nl} \sim \frac{\ell}{\delta U_\ell}$$

A velocity difference across the eddy changes its shape over this time. Numerical factors associated with a circular orbit are not retained.

Figure 4: A velocity difference across a length estimates intrinsic deformation. Uniform sweeping carries a structure along without distorting it.

Energy per unit mass at scale ℓ is of order δU_ℓ^2. A common transfer rate therefore gives

$$\varepsilon \sim \frac{\delta U_\ell^2}{\tau_{\rm cas}} \sim \frac{\delta U_\ell^3}{\ell}, \qquad \boxed{\delta U_\ell \sim (\varepsilon \ell)^{1/3}, \quad \tau_{\rm nl} \sim \varepsilon^{-1/3}\ell^{2/3}.} \tag{3.2}$$

Smaller scales contain less energy and process that energy faster. Constant flux means the same average throughput, rather than the same amount of energy at every scale.

3.2 From an amplitude to the spectrum

Consider a logarithmic band of wavenumbers around k. Its width is of order k, so its energy is of order $kE_U(k)$. For an inertial-range power law, fluctuations at $\ell \sim k^{-1}$ give the estimate

$$\delta U_\ell^2 \sim kE_U(k), \qquad k \sim \ell^{-1}. \tag{3.3}$$

Insert the K41 amplitude and divide by k:

$$\boxed{E_U(k) \sim \varepsilon^{2/3}k^{-5/3}.} \tag{3.4}$$

This relation is a scale estimate; it does not assert that a velocity increment contains just one Fourier mode.

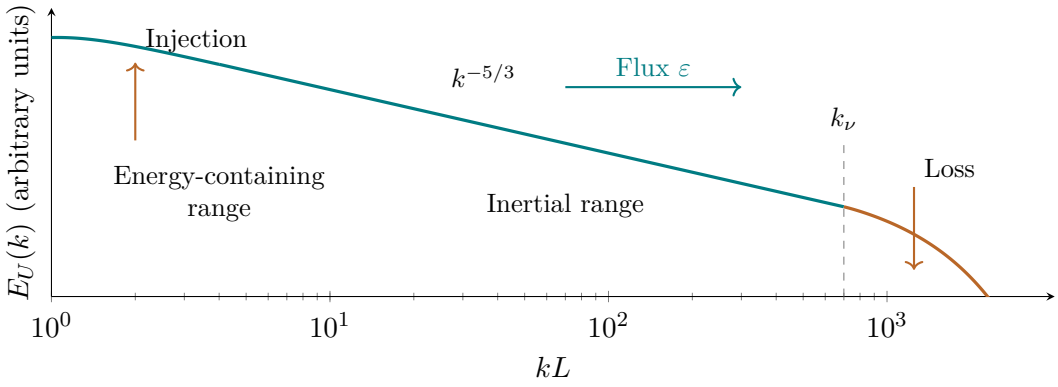


Figure 5: A schematic K41 energy spectrum. The forcing range and cutoff shape are illustrative; the inertial-range slope follows from the nonlinear transfer-time estimate.

3.3 The cutoff, the cascade time, and locality

Viscosity matters when its smoothing time matches the nonlinear time:

$$\frac{\ell_\nu^2}{\nu} \sim \varepsilon^{-1/3}\ell_\nu^{2/3} \quad \Longrightarrow \quad \ell_\nu \sim (\nu^3/\varepsilon)^{1/4}, \qquad \frac{\ell_\nu}{L} \sim {\rm Re}^{-3/4}. \tag{3.5}$$

The last relation uses the outer-scale flux estimate $\varepsilon \sim U_L^3/L$. Below the viscous cutoff the velocity field is smooth, so sufficiently small increments become proportional to separation.

How long does energy take to reach the small scales? Since $\tau_{\mathrm{nl}} \propto \ell^{2/3}$, each fixed decrease in scale produces a shorter transfer time. Most of the transit time is spent near the outer scale; the smaller-scale steps add progressively less. The natural estimate is a few outer-scale turnover times. The transient also depends on the initial state and forcing.

The same scaling helps motivate locality. A much larger eddy mainly sweeps a small one along; its strain rate is smaller than the small eddy's own characteristic strain. Much smaller fluctuations can be rapid but act over short distances and partially cancel across a larger structure. Comparable scales can therefore dominate the net transfer. This is the physical basis of the local-cascade estimate, rather than a claim that interactions between distant scales vanish.

What produced the $-5/3$ law?

A common energy flux plus the estimate $\tau_{\mathrm{cas}} \sim \ell/\delta U_\ell$ fixes the amplitude and spectrum. To change the spectrum, look for a process that changes the transfer time or the relation between geometry and amplitude.

4 What the magnetic field adds

4.1 The MHD equations and the magnetic force

With scalar pressure and magnetic diffusivity η, the MHD equations are

$$\partial_t \rho + \boldsymbol{\nabla} \cdot (\rho \boldsymbol{U}) = 0, \tag{4.1}$$

$$\rho \frac{\mathrm{D}}{\mathrm{D}t}\boldsymbol{U} = -\boldsymbol{\nabla} p + \frac{(\boldsymbol{\nabla} \times \boldsymbol{B}) \times \boldsymbol{B}}{4\pi}, \tag{4.2}$$

$$\partial_t \boldsymbol{B} = \boldsymbol{\nabla} \times (\boldsymbol{U} \times \boldsymbol{B}) + \eta \nabla^2 \boldsymbol{B}, \qquad \boldsymbol{\nabla} \cdot \boldsymbol{B} = 0. \tag{4.3}$$

An equation of state or pressure evolution closes this system. For example, adiabatic ideal MHD has $\mathrm{D}(p/\rho^\gamma)/\mathrm{D}t = 0$. We will use constant-density, incompressible MHD for the turbulence and invariant calculations; the broader equations clarify what magnetic and compressive effects exist.

Split the magnetic force into pressure and tension:

$$\frac{(\boldsymbol{\nabla} \times \boldsymbol{B}) \times \boldsymbol{B}}{4\pi} = -\boldsymbol{\nabla} \frac{B^2}{8\pi} + \frac{\boldsymbol{B} \cdot \boldsymbol{\nabla} \boldsymbol{B}}{4\pi}. \tag{4.4}$$

Magnetic pressure resists field-strength variations, while tension resists bending. For a curved field, the curvature part of the tension points toward the centre of curvature. These effects allow magnetic energy to exchange with kinetic energy and introduce a preferred direction for the response.

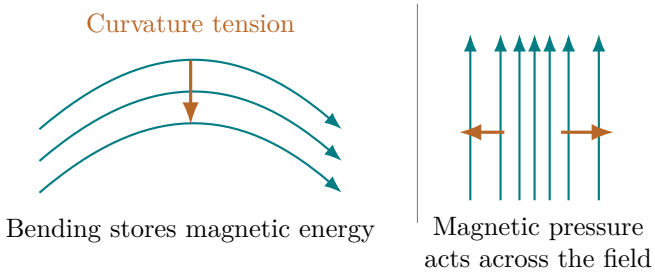


Figure 6: Magnetic curvature tension and magnetic pressure. The drawings show force contributions; other forces can balance them.

4.2 Stretching and flux freezing

Combining ideal induction and mass conservation gives

$$\frac{\mathrm{D}}{\mathrm{D}t}\left(\frac{\boldsymbol{B}}{\rho}\right) = \left(\frac{\boldsymbol{B}}{\rho}\cdot\boldsymbol{\nabla}\right)\boldsymbol{U}. \tag{4.5}$$

For incompressible flow this becomes $\mathrm{D}\boldsymbol{B}/\mathrm{D}t = \boldsymbol{B}\cdot\boldsymbol{\nabla}\boldsymbol{U}$: velocity gradients stretch and rotate the field. In compressible flow, compression also changes its strength.

The corresponding integral statement is conservation of magnetic flux through a material surface in ideal MHD:

$$\Phi = \int_{S(t)} \boldsymbol{B}\cdot\mathrm{d}\boldsymbol{S}, \qquad \frac{\mathrm{d}\Phi}{\mathrm{d}t} = 0. \tag{4.6}$$

The surface can change area and orientation while its flux remains constant. Finite resistivity can matter in thin current sheets even when the outer magnetic Reynolds number is large.

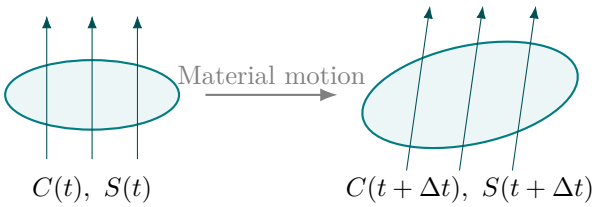


Figure 7: Ideal flux freezing applies to a loop and surface carried by the fluid. The area, orientation, and field strength can change while the enclosed flux remains constant.

4.3 Alfvén waves and anisotropy

Take a uniform guide field $\boldsymbol{B}_0 = B_0\boldsymbol{e}_\parallel$ and define $v_\mathrm{A} = B_0/\sqrt{4\pi\rho_0}$. Small transverse disturbances obey

$$\partial_t\delta\boldsymbol{U}_\perp = \frac{B_0}{4\pi\rho_0}\partial_\parallel\delta\boldsymbol{B}_\perp, \qquad \partial_t\delta\boldsymbol{B}_\perp = B_0\partial_\parallel\delta\boldsymbol{U}_\perp. \tag{4.7}$$

Combining them gives

$$\partial_t^2\delta\boldsymbol{U}_\perp = v_\mathrm{A}^2\partial_\parallel^2\delta\boldsymbol{U}_\perp, \qquad \omega = \pm v_\mathrm{A}k_\parallel. \tag{4.8}$$

A propagating Alfvén wave has equal velocity and magnetic amplitudes when the magnetic amplitude is expressed in velocity units: $\delta U_\perp = \delta B_\perp/\sqrt{4\pi\rho_0}$. Magnetic tension communicates transverse disturbances along the field. Compressive motions have additional gas and magnetic restoring forces, illustrated below; the cascade model developed next focuses on the Alfvénic part.

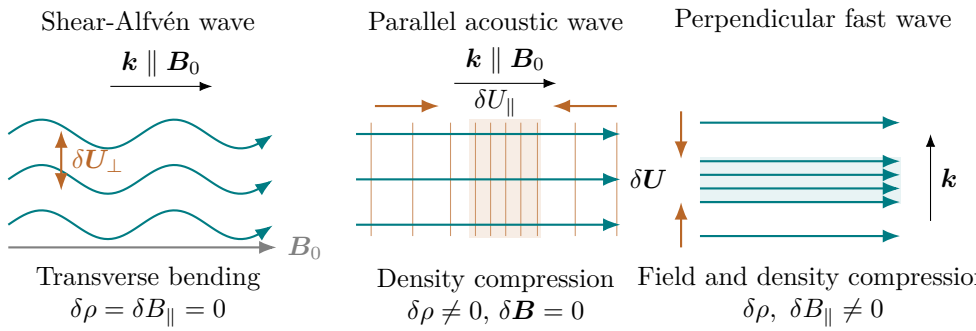


Figure 8: Three wave geometries: transverse field-line bending, parallel gas compression, and perpendicular gas-and-field compression. These special directions illustrate the restoring forces.

A magnetic field therefore distinguishes parallel propagation from transverse distortion. We must allow separate lengths $\ell_\parallel$ and $\ell_\perp$, rather than assume a spherical eddy. At sufficiently small scales of a strong cascade, the relevant parallel direction is the *local* field seen by that fluctuation.

The new ingredient

Hydrodynamic straining still exists, but an Alfvénic fluctuation can also propagate. Its lifetime and shape must be determined by comparing these two processes.

5 Weak and strong turbulence

5.1 Two times and the strength of an encounter

For primarily transverse Alfvénic fluctuations, use the physical estimates

$$\tau_\mathrm{A} \sim \frac{\ell_\parallel}{v_\mathrm{A}}, \qquad \tau_\mathrm{nl} \sim \frac{\ell_\perp}{\delta U_\ell}, \qquad \chi \equiv \frac{\tau_\mathrm{A}}{\tau_\mathrm{nl}} \sim \frac{\delta U_\ell \ell_\parallel}{v_\mathrm{A} \ell_\perp}. \tag{5.1}$$

The perpendicular length enters because the transverse flow strains the transverse structure. These are estimates for the Alfvénic geometry we are studying, not a replacement of the full MHD equations. We initially take comparable amplitudes of the two propagation directions and no additional alignment suppression.

When $\chi \ll 1$, propagation carries a packet through an encounter before nonlinear distortion becomes appreciable: the turbulence is weak. When $\chi \sim 1$, order-unity distortion can occur over a propagation time: the interaction is strong. If the distortion is initially much faster, the assumed coherent packet cannot remain unchanged over its proposed parallel extent.

Small amplitude relative to v_A does not by itself imply weak turbulence. An elongated fluctuation can have $\delta U_\ell / v_\mathrm{A} \ll 1$ and still satisfy $\chi \sim 1$.

5.2 The weak-cascade baseline

In the classical balanced weak-cascade picture, many small, approximately decorrelated changes accumulate before a packet loses its identity.

The nonlinear rate of change of a packet is estimated as

$$\left| \frac{\mathrm{d}\,\delta \boldsymbol{U}_\ell}{\mathrm{d}t} \right|_\mathrm{nl} \sim \frac{\delta U_\ell^2}{\ell_\perp} = \frac{\delta U_\ell}{\tau_\mathrm{nl}}.$$

Thus $\tau_{\rm nl}$ is the time for order-unity distortion if the same straining persists. An encounter with a counterpropagating packet lasts only $\tau_{\rm A} \sim \ell_\parallel / v_{\rm A}$. In weak turbulence, $\tau_{\rm A} \ll \tau_{\rm nl}$, so the change $\Delta U_{\rm one}$ in one encounter is small:

$$\frac{\Delta U_{\rm one}}{\delta U_\ell} \sim \frac{\tau_{\rm A}}{\tau_{\rm nl}} = \chi \ll 1.$$

If successive changes are approximately uncorrelated, their typical accumulated size grows as a random walk:

$$\frac{\Delta U_{\rm total}}{\delta U_\ell} \sim \sqrt{N}\,\chi.$$

A cascade time corresponds to order-unity distortion of the original packet. Hence

$$\sqrt{N}\,\chi \sim 1 \quad \Longrightarrow \quad N \sim \chi^{-2}, \qquad \boxed{\tau_{\rm cas} \sim N\tau_{\rm A} \sim \frac{\tau_{\rm A}}{\chi^2} = \frac{\tau_{\rm nl}^2}{\tau_{\rm A}}.}$$

The resulting cascade time and perpendicular spectrum are

$$\tau_{\rm cas} \sim \frac{\tau_{\rm nl}^2}{\tau_{\rm A}}, \qquad \delta U_\ell \propto \ell_\perp^{1/2}, \qquad E_\perp(k_\perp) \propto k_\perp^{-2}. \tag{5.2}$$

These results assume that the propagating fluctuations retain approximately the same parallel scale while their perpendicular scale decreases [6]. We use them here as a reference regime; the statistical and resonant-interaction derivation is beyond the present discussion.

At fixed $\ell_\parallel$, this weak-cascade scaling gives $\chi \propto \ell_\perp^{-1/2}$. The amplitude decreases down the cascade, but the perpendicular gradient grows fast enough that the interaction strengthens. If the cascade reaches $\chi \sim 1$ before dissipation or kinetic effects intervene, it can enter a strong regime. The next section develops that regime directly.

6 Critical balance and the GS95 cascade

6.1 Critical balance as a physical hypothesis

A transverse pattern changes over $\tau_{\rm nl}$, while Alfvén signals communicate that pattern along the field at speed $v_{\rm A}$. A parallel coherence length much larger than $v_{\rm A}\tau_{\rm nl}$ would require communication over a distance the signal cannot traverse before the pattern changes. This motivates a strong state with

$$\boxed{\tau_{\rm A} \sim \tau_{\rm nl}, \qquad \frac{\ell_\parallel}{v_{\rm A}} \sim \frac{\ell_\perp}{\delta U_\ell}.} \tag{6.1}$$

This is the critical-balance hypothesis. The communication argument motivates it; it does not prove equality of the times for every fluctuation.

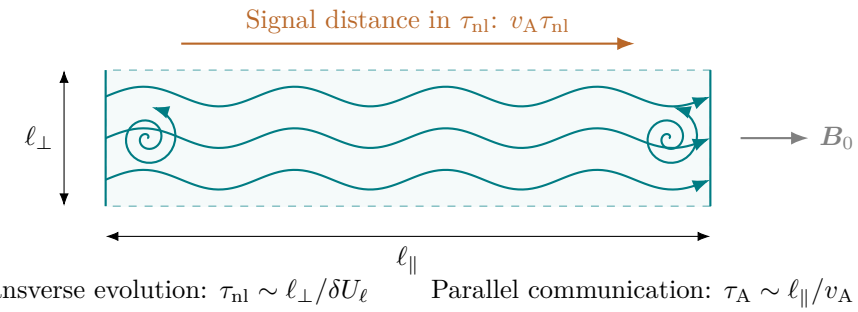


Figure 9: Parallel communication during a nonlinear lifetime motivates critical balance. This is a physical coherence argument rather than a proof for every fluctuation.

6.2 Amplitude, spectrum, and anisotropy

The GS95 baseline considers strong, approximately balanced Alfvénic turbulence, with $\delta U_\ell \sim \delta B_\ell/\sqrt{4\pi\rho_0}$, and takes the cascade time to be the nonlinear distortion time [5]:

$$\tau_{\rm cas} \sim \tau_{\rm nl} \sim \tau_{\rm A}, \qquad \varepsilon \sim \frac{\delta U_\ell^3}{\ell_\perp}. \tag{6.2}$$

The amplitude and perpendicular spectrum follow by the same short argument used in HD:

$$\boxed{\delta U_\ell \sim (\varepsilon \ell_\perp)^{1/3}, \qquad E_\perp(k_\perp) \sim \varepsilon^{2/3} k_\perp^{-5/3}.} \tag{6.3}$$

Here $E_\perp$ is the one-dimensional perpendicular spectrum after integrating over the other wavevector coordinates; $\delta U_\ell^2 \sim k_\perp E_\perp(k_\perp)$ in scaling. The $-5/3$ exponent resembles K41, but the geometry differs.

Critical balance supplies that geometry:

$$\boxed{\ell_\parallel \sim v_{\rm A} \varepsilon^{-1/3} \ell_\perp^{2/3}, \qquad \frac{\ell_\parallel}{\ell_\perp} \propto \ell_\perp^{-1/3}.} \tag{6.4}$$

Smaller eddies are more elongated relative to their transverse size. Both lengths decrease down the cascade; the perpendicular length decreases faster.

Critical balance also predicts the spectrum along the *local* magnetic field. Let $\delta U_{\ell_\parallel}$ denote the fluctuation across a parallel separation $\ell_\parallel$; the subscript labels the separation, not a velocity component. Using $\tau_{\rm cas} \sim \ell_\parallel/v_{\rm A}$,

$$\varepsilon \sim \frac{\delta U_{\ell_\parallel}^2}{\ell_\parallel/v_{\rm A}} \quad \Longrightarrow \quad \delta U_{\ell_\parallel}^2 \sim \frac{\varepsilon}{v_{\rm A}} \ell_\parallel. \tag{6.5}$$

As before, energy in a logarithmic band is $\delta U_{\ell_\parallel}^2 \sim k_\parallel E_\parallel(k_\parallel)$ at $k_\parallel \sim \ell_\parallel^{-1}$. Hence

$$\boxed{E_\parallel(k_\parallel) \sim \frac{\varepsilon}{v_{\rm A}} k_\parallel^{-2}, \qquad \text{parallel spectral index} = -2.} \tag{6.6}$$

This is a local-field parallel spectrum; using a single global field direction can mix parallel and perpendicular structure and hide this scaling.

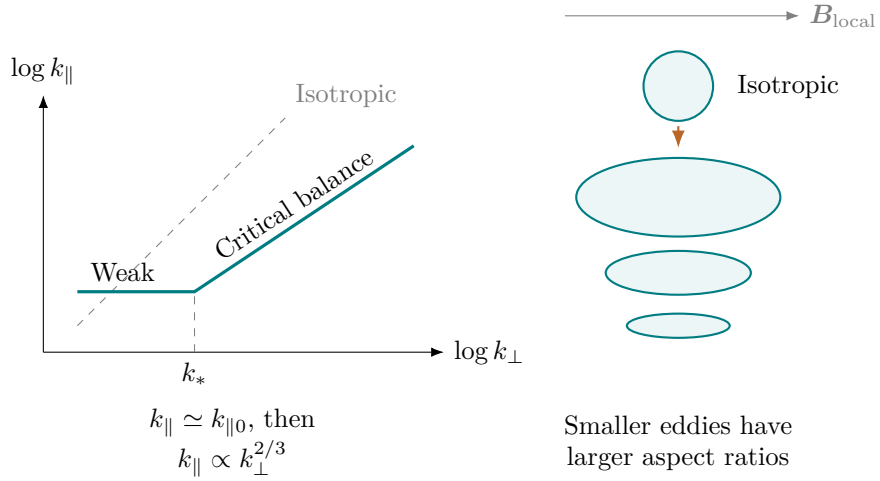


Figure 10: Weak-to-strong transition and local GS95 anisotropy. Both eddy dimensions decrease, while their aspect ratio increases toward smaller scales.

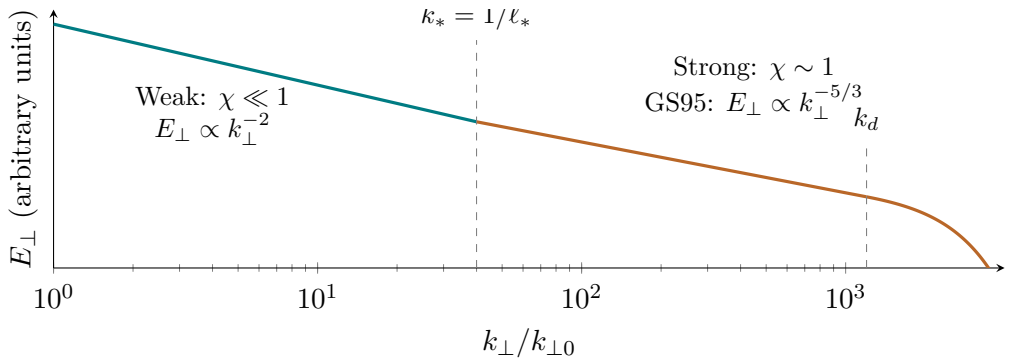


Figure 11: A schematic weak-to-strong cascade. The strong-range slope uses the GS95 transfer-time estimate; the cutoff marks the end of the assumed fluid cascade.

6.3 How far can this model be continued?

If the same coupled cascade reaches collisional diffusion scales, comparison with $\ell_\perp^2/\nu$ or $\ell_\perp^2/\eta$ gives

$$\ell_{\nu,\perp} \sim (\nu^3/\varepsilon)^{1/4}, \qquad \ell_{\eta,\perp} \sim (\eta^3/\varepsilon)^{1/4}. \tag{6.7}$$

For a dimensionless form, take $L_\perp$ and U_L at the outer edge of the *strong* cascade, so that $\varepsilon \sim U_L^3/L_\perp$. Define

$$\mathrm{Re}_L = \frac{U_L L_\perp}{\nu}, \qquad \mathrm{Rm}_L = \frac{U_L L_\perp}{\eta}. \tag{6.8}$$

Substitution immediately gives the perpendicular viscous and resistive scales:

$$\boxed{\frac{\ell_{\nu,\perp}}{L_\perp} \sim \mathrm{Re}_L^{-3/4}, \qquad \frac{\ell_{\eta,\perp}}{L_\perp} \sim \mathrm{Rm}_L^{-3/4}.} \tag{6.9}$$

If the original forcing drives a weak cascade, $L_\perp$ here refers to the transition into the strong range, rather than automatically to the forcing scale.

This continuation is simplest for Pm of order unity. At extreme Pm, one field may become smooth while the other retains finer structure. In weakly collisional plasmas, particle scales can intervene earlier and require a kinetic description.

A baseline to examine

We have obtained a spectrum by combining a mean energy flux, a transfer-time estimate, and a geometry hypothesis. We now return to the MHD equations to ask what else is conserved, what interacts with what, and how those facts can modify the cascade.

7 Quadratic invariants and selective decay

For constant density ρ_0, express the magnetic field in velocity units and normalize the other quantities consistently:

Normalization used from Section 7 onward

$$\begin{aligned} \boldsymbol{B} &\equiv \frac{\boldsymbol{B}_{\text{physical}}}{\sqrt{4\pi\rho_0}}, & \boldsymbol{A} &\equiv \frac{\boldsymbol{A}_{\text{physical}}}{\sqrt{4\pi\rho_0}}, \\ E &\equiv \frac{E_{\text{physical}}}{\rho_0}, & H_c &\equiv \frac{H_{c,\text{physical}}}{\sqrt{4\pi\rho_0}}, \\ H_m &\equiv \frac{H_{m,\text{physical}}}{4\pi\rho_0}, & \Phi &\equiv \frac{\Phi_{\text{physical}}}{\sqrt{4\pi\rho_0}}. \end{aligned} \tag{7.1}$$

The velocity $\boldsymbol{U}$ is unchanged. Both $\boldsymbol{U}$ and $\boldsymbol{B}$ have velocity units. All fields, fluxes, energies, and helicities below use these normalized quantities.

The normalized energy and cross helicity are

$$E = \frac{1}{2}\int_V (U^2 + B^2)\,\mathrm{d}V, \qquad H_c = \int_V \boldsymbol{U}\cdot\boldsymbol{B}\,\mathrm{d}V. \tag{7.2}$$

The integrals remain volume integrals: E/V is the energy per unit mass. The same energy normalization applies to E_B. Scaling $\boldsymbol{A}$ and Φ with $\boldsymbol{B}$, and H_m with its square, preserves $\boldsymbol{B} = \boldsymbol{\nabla}\times\boldsymbol{A}$ and the flux-linkage formulas.

The ideal invariants identify what nonlinear motion can redistribute without changing its volume integral. They also help explain why a weakly dissipative plasma may relax toward an organized state. These are distinct uses: ideal conservation is exact, whereas a proposed relaxation requires assumptions about which quantities decay most slowly.

We use the total fields $\boldsymbol{U}$ and $\boldsymbol{B}$, set forcing to zero, and use periodic boundaries or boundaries that remove the corresponding surface terms.

For reference, the governing equations are

$$\partial_t\boldsymbol{U} + (\boldsymbol{U}\cdot\boldsymbol{\nabla})\boldsymbol{U} = -\boldsymbol{\nabla}\Pi + (\boldsymbol{B}\cdot\boldsymbol{\nabla})\boldsymbol{B} + \nu\nabla^2\boldsymbol{U}, \tag{7.3}$$

$$\partial_t\boldsymbol{B} + (\boldsymbol{U}\cdot\boldsymbol{\nabla})\boldsymbol{B} = (\boldsymbol{B}\cdot\boldsymbol{\nabla})\boldsymbol{U} + \eta\nabla^2\boldsymbol{B}, \tag{7.4}$$

$$\boldsymbol{\nabla}\cdot\boldsymbol{U} = \boldsymbol{\nabla}\cdot\boldsymbol{B} = 0. \tag{7.5}$$

Here Π is the total pressure per unit mass, including the magnetic contribution $B^2/2$; ν is the kinematic viscosity and η is the magnetic diffusivity. Define

$$\boldsymbol{\omega} = \boldsymbol{\nabla}\times\boldsymbol{U}, \qquad \boldsymbol{j} = \boldsymbol{\nabla}\times\boldsymbol{B}. \tag{7.6}$$

The symbol $\boldsymbol{j}$ denotes the curl of the normalized magnetic field.

The three integral budgets are collected below, with $\boldsymbol{B} = \boldsymbol{\nabla}\times\boldsymbol{A}$. For all three, remove the corresponding boundary fluxes; for magnetic helicity, the vector potential must also obey the conditions discussed below.

Three integral budgets

$$\frac{\mathrm{d}E}{\mathrm{d}t} = \frac{\mathrm{d}}{\mathrm{d}t}\left[\frac{1}{2}\int_V (U^2 + B^2)\,\mathrm{d}V\right] = -\nu\int_V \omega^2\,\mathrm{d}V - \eta\int_V j^2\,\mathrm{d}V$$

$$\frac{\mathrm{d}H_m}{\mathrm{d}t} = \frac{\mathrm{d}}{\mathrm{d}t}\int_V \boldsymbol{A}\cdot\boldsymbol{B}\,\mathrm{d}V = -2\eta\int_V \boldsymbol{j}\cdot\boldsymbol{B}\,\mathrm{d}V$$

$$\frac{\mathrm{d}H_c}{\mathrm{d}t} = \frac{\mathrm{d}}{\mathrm{d}t}\int_V \boldsymbol{U}\cdot\boldsymbol{B}\,\mathrm{d}V = -(\eta+\nu)\int_V \boldsymbol{j}\cdot\boldsymbol{\omega}\,\mathrm{d}V$$

With $\nu = \eta = 0$, all three time derivatives vanish.

7.1 Magnetic helicity: definition and gauge invariance

Use the normalized magnetic field $\boldsymbol{B}$ and a vector potential $\boldsymbol{A}$ satisfying $\boldsymbol{B} = \boldsymbol{\nabla}\times\boldsymbol{A}$. Magnetic helicity is

$$\boxed{H_m = \int_V \boldsymbol{A}\cdot\boldsymbol{B}\,\mathrm{d}V.} \tag{7.7}$$

The vector potential is not unique: adding the gradient of a smooth, single-valued scalar χ leaves $\boldsymbol{B}$ unchanged. Under $\boldsymbol{A}\to\boldsymbol{A}+\boldsymbol{\nabla}\chi$, the change in helicity is

$$\begin{aligned} H_m' - H_m &= \int_V \boldsymbol{B}\cdot\boldsymbol{\nabla}\chi\,\mathrm{d}V \\ &= \int_V \boldsymbol{\nabla}\cdot(\chi\boldsymbol{B})\,\mathrm{d}V = \oint_{\partial V}\chi\boldsymbol{B}\cdot\mathrm{d}\boldsymbol{S}. \end{aligned} \tag{7.8}$$

Here we used $\boldsymbol{\nabla}\cdot\boldsymbol{B} = 0$. If the field is tangent to the boundary, $\boldsymbol{B}\cdot\boldsymbol{n} = 0$, this surface term vanishes: H_m is *gauge invariant*. The local quantity $\boldsymbol{A}\cdot\boldsymbol{B}$ need not be gauge invariant; it is the integral over a closed magnetic volume that has this property.

A periodic domain with zero net magnetic flux also admits a periodic vector potential and a gauge-invariant H_m. We use these closed or periodic conditions below; an open magnetic system requires additional boundary accounting. Gauge invariance makes H_m well defined. Conservation is a separate statement, obtained from its evolution equation.

7.2 What can survive while energy decays?

At finite diffusivity, the energy and both helicities have the budgets stated above. Cross-helicity loss is not sign definite, and approximate cross-helicity conservation during decay is an additional physical assumption.

Magnetic helicity has a stronger basis for selective decay. The resistive loss of magnetic energy is

$$\left.\frac{\mathrm{d}E_B}{\mathrm{d}t}\right|_{\text{resistive}} = -\eta\int_V |\boldsymbol{\nabla}\times\boldsymbol{B}|^2\,\mathrm{d}V, \qquad E_B = \frac{1}{2}\int_V B^2\,\mathrm{d}V. \tag{7.9}$$

Energy loss contains two factors of the field gradient; helicity loss contains only one. More precisely,

$$\left|\frac{\mathrm{d}H_m}{\mathrm{d}t}\right| \le 2\eta\left(\int_V B^2\,\mathrm{d}V\right)^{1/2}\left(\int_V |\boldsymbol{\nabla}\times\boldsymbol{B}|^2\,\mathrm{d}V\right)^{1/2}. \tag{7.10}$$

If magnetic energy and its resistive loss rate remain bounded as $\eta\to 0$, this bound tends to zero at least as fast as $\eta^{1/2}$. Sharp current structures can therefore dissipate a finite amount of energy per unit time

while changing H_m very slowly. This motivates relaxation toward lower magnetic energy at nearly fixed helicity [10].

Keep three statements separate

Gauge invariance makes the magnetic helicity well defined. Ideal conservation follows from its evolution equation and the boundary conditions. Selective decay means that helicity remains nearly fixed while energy is dissipated.

We first follow the magnetic-helicity constraint to its topological meaning and the Taylor state. We will then return to cross helicity and the relation between velocity and magnetic fluctuations.

8 Magnetic helicity: flux linkage and Taylor relaxation

8.1 Magnetic flux and the meaning of helicity

To understand what magnetic-helicity conservation constrains, return to the physical meaning of

$$H_m = \int_V \boldsymbol{A}\cdot\boldsymbol{B}\,\mathrm{d}V, \qquad \boldsymbol{B} = \boldsymbol{\nabla}\times\boldsymbol{A}. \tag{8.1}$$

Magnetic energy measures field strength. Helicity also tells us how magnetic field lines are linked. To see this, consider closed magnetic flux tubes contained inside the volume, with no magnetic flux crossing the outer boundary.

A flux tube is bounded by a surface tangent to $\boldsymbol{B}$. Its magnetic flux through a cross-section S is

$$\Phi = \int_S \boldsymbol{B}\cdot\mathrm{d}\boldsymbol{S}. \tag{8.2}$$

Since $\boldsymbol{\nabla}\cdot\boldsymbol{B}=0$, every cross-section carries the same flux. Ideal flux freezing preserves Φ as the tube moves and deforms. It also preserves the linkage of the tubes: they cannot pass through one another without reconnection.

8.2 Two linked flux tubes

Take two thin, untwisted closed tubes carrying fluxes Φ_1 and Φ_2, linked once with positive orientation as in figure 12. We neglect self-helicity in this two-tube calculation.

Write $\boldsymbol{B}=B\hat{\boldsymbol{b}}$, $\mathrm{d}\boldsymbol{l}=\hat{\boldsymbol{b}}\,\mathrm{d}l$, and $\mathrm{d}\boldsymbol{S}=\hat{\boldsymbol{b}}\,\mathrm{d}S$. In the thin-tube limit, the helicity of T_1 is

$$\begin{aligned}
H_1 &= \int_{T_1}\mathrm{d}V\,\boldsymbol{A}\cdot\boldsymbol{B} = \int_{T_1}\underbrace{\mathrm{d}\boldsymbol{l}}_{\hat{\boldsymbol{b}}\,\mathrm{d}l}\cdot\underbrace{\mathrm{d}\boldsymbol{S}}_{\hat{\boldsymbol{b}}\,\mathrm{d}S}\,\boldsymbol{A}\cdot\hat{\boldsymbol{b}}\,B \\
&= \int_{T_1}\boldsymbol{A}\cdot\hat{\boldsymbol{b}}\,\mathrm{d}l\,B\hat{\boldsymbol{b}}\cdot\hat{\boldsymbol{b}}\,\mathrm{d}S \\
&= \int_{T_1}\boldsymbol{A}\cdot\mathrm{d}\boldsymbol{l}\,\boldsymbol{B}\cdot\mathrm{d}\boldsymbol{S} \\
&= \Phi_1 \underbrace{\int_{T_1}\boldsymbol{A}\cdot\mathrm{d}\boldsymbol{l}}_{\int_{S_1}\boldsymbol{B}\cdot\mathrm{d}\boldsymbol{S}} = \Phi_1\Phi_2. \\
&= \Phi_{\text{hole in }T_1} = \Phi_2
\end{aligned} \tag{8.3}$$

The cross-sectional flux is Φ_1. In the last step, the line integral runs once around T_1; Stokes' theorem gives the flux through its hole, spanned by S_1. Tube 2 threads that hole once, so this flux is Φ_2.

The same argument for tube 2 gives $H_2 = \Phi_2\Phi_1$. Adding both contributions,

$$\boxed{H_m = H_1 + H_2 = 2\Phi_1\Phi_2.} \tag{8.4}$$

Now consider many thin, closed tubes carrying fluxes Φ_i, neglecting self-helicity for now. Let n_{ij} be the *signed linking number*: the net number of times tube j passes through a surface spanning the hole of tube i. With consistent curve orientations and signed fluxes, Stokes' theorem gives

$$H_i = \Phi_i \int_{T_i} \boldsymbol{A} \cdot \mathrm{d}\boldsymbol{l} = \Phi_i \sum_{j\neq i} n_{ij}\Phi_j.$$

Adding the contributions of all the tubes,

$$\boxed{H_m = \sum_i \sum_{j\neq i} \Phi_i\Phi_j n_{ij} = 2\sum_{i<j} \Phi_i\Phi_j n_{ij}.} \tag{8.5}$$

Since $n_{ij} = n_{ji}$, each pair contributes twice: once in H_i and once in H_j, recovering equation (8.4) when $n_{12} = 1$. Thus *magnetic helicity measures the number of linkages between flux tubes, weighted by their magnetic fluxes and counted with sign.*

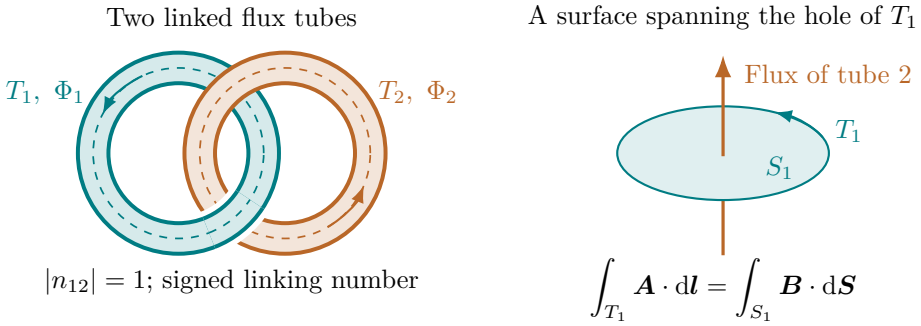


Figure 12: A linked pair and the flux counted by Stokes' theorem. Over–under crossings indicate two disjoint tubes in three dimensions. The surface S_1 spans the loop's hole; it is not a cross-section of tube 1. Each tube contributes the same product of fluxes to the helicity.

This is the *topological meaning* of magnetic helicity: it measures linkage weighted by magnetic flux. Smooth ideal deformations change the tubes' shapes but preserve their fluxes and linkage, hence their helicity. Opposite signed contributions can cancel, so H_m is not a complete description of every detail of the topology.

8.3 Twist and reconnection

A separate second tube is not necessary for nonzero helicity. Field lines inside a single twisted tube can link one another. Figure 13 shows this internal winding: the same flux-linkage interpretation applies to the smaller bundles of field lines within the tube.

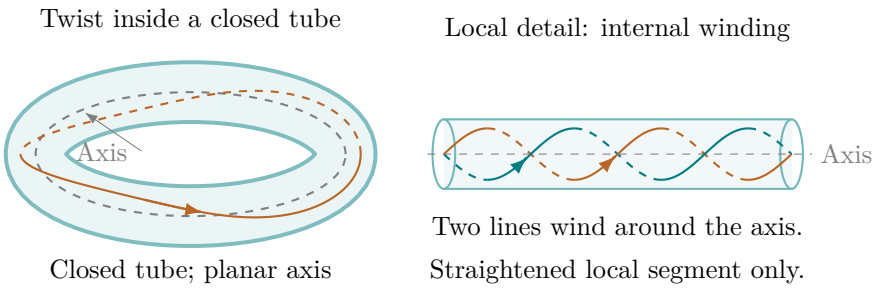


Figure 13: Self helicity from internal winding. Left: a closed toroidal tube with a planar axis and one neighbouring field line. Right: a straightened local segment shows two neighbouring lines winding around the dashed axis; its cut ends do not represent an open magnetic system. Dashed parts of the helices lie behind the axis.

Reconnection can change which tubes are linked and can convert linkage between tubes into twist within the products. These geometrical contributions can change even when the total helicity changes very little. This is an approximate statement at high conductivity, not exact conservation at finite resistivity: with no boundary flux,

$$\frac{\mathrm{d}H_m}{\mathrm{d}t} = -2\eta \int_V \boldsymbol{B}\cdot(\boldsymbol{\nabla}\times\boldsymbol{B})\,\mathrm{d}V.$$

The selective-decay argument in section 7 explains how sharp current structures can dissipate magnetic energy while leaving H_m nearly fixed. Reconnection relaxes detailed topological constraints, while this surviving global constraint limits the final state.

8.4 Minimum magnetic energy at fixed helicity

Without a constraint, the minimum magnetic energy is the zero field. A retained nonzero H_m prevents that outcome. Seek a minimum of the normalized magnetic energy

$$E_B = \frac{1}{2}\int_V B^2\,\mathrm{d}V \tag{8.6}$$

at fixed magnetic helicity. Let $H_{m,0}$ denote its prescribed value. Equivalently, minimize $2E_B = \int_V B^2\,\mathrm{d}V$; multiplying the energy by a constant does not change the minimizing field. With a constant Lagrange multiplier α, the constrained stationarity condition is

$$\delta\left[\int_V \left(B^2 - \alpha\boldsymbol{A}\cdot\boldsymbol{B}\right)\mathrm{d}V + \alpha H_{m,0}\right] = 0. \tag{8.7}$$

Variation with respect to α imposes $\int_V \boldsymbol{A}\cdot\boldsymbol{B}\,\mathrm{d}V = H_{m,0}$. In the field variation, α is held fixed, so $\alpha H_{m,0}$ contributes zero. Here δ denotes a variation between nearby field configurations.

Both fields change. Since $\boldsymbol{B} = \boldsymbol{\nabla}\times\boldsymbol{A}$, their variations satisfy

$$\delta\boldsymbol{B} = \boldsymbol{\nabla}\times\delta\boldsymbol{A}.$$

Keep $\delta\boldsymbol{B}$ explicit in the first step, then substitute this relation. For twice the magnetic energy,

$$\begin{aligned}
\delta\int_V B^2\,\mathrm{d}V &= 2\int_V \boldsymbol{B}\cdot\delta\boldsymbol{B}\,\mathrm{d}V \\
&= 2\int_V \boldsymbol{B}\cdot(\boldsymbol{\nabla}\times\delta\boldsymbol{A})\,\mathrm{d}V \\
&= 2\int_V \left[-\boldsymbol{\nabla}\cdot(\boldsymbol{B}\times\delta\boldsymbol{A}) + (\boldsymbol{\nabla}\times\boldsymbol{B})\cdot\delta\boldsymbol{A}\right]\mathrm{d}V \\
&= -2\oint_{\partial V}(\boldsymbol{B}\times\delta\boldsymbol{A})\cdot\mathrm{d}\boldsymbol{S} + 2\int_V (\boldsymbol{\nabla}\times\boldsymbol{B})\cdot\delta\boldsymbol{A}\,\mathrm{d}V.
\end{aligned} \tag{8.8}$$

For magnetic helicity, vary both factors in $\boldsymbol{A}\cdot\boldsymbol{B}$:

$$\begin{aligned}\delta H_m &= \int_V [\boldsymbol{B}\cdot\delta\boldsymbol{A} + \boldsymbol{A}\cdot\delta\boldsymbol{B}]\,\mathrm{d}V \\ &= \int_V [\boldsymbol{B}\cdot\delta\boldsymbol{A} + \boldsymbol{A}\cdot(\boldsymbol{\nabla}\times\delta\boldsymbol{A})]\,\mathrm{d}V \\ &= \int_V [\boldsymbol{B}\cdot\delta\boldsymbol{A} - \boldsymbol{\nabla}\cdot(\boldsymbol{A}\times\delta\boldsymbol{A}) + (\boldsymbol{\nabla}\times\boldsymbol{A})\cdot\delta\boldsymbol{A}]\,\mathrm{d}V \\ &= -\oint_{\partial V}(\boldsymbol{A}\times\delta\boldsymbol{A})\cdot\mathrm{d}\boldsymbol{S} + 2\int_V \boldsymbol{B}\cdot\delta\boldsymbol{A}\,\mathrm{d}V. \end{aligned} \tag{8.9}$$

The last line uses $\boldsymbol{\nabla}\times\boldsymbol{A}=\boldsymbol{B}$: the two varied factors give equal volume contributions.

Take variations that preserve the boundary data and remove these surface terms, for example by fixing the tangential part of $\boldsymbol{A}$ at the boundary. The interior variations remain free. Then

$$2\int_V (\boldsymbol{\nabla}\times\boldsymbol{B} - \alpha\boldsymbol{B})\cdot\delta\boldsymbol{A}\,\mathrm{d}V = 0 \tag{8.10}$$

for every allowed interior variation, which requires

$$\boxed{\boldsymbol{\nabla}\times\boldsymbol{B} = \alpha\boldsymbol{B}, \qquad \alpha = \text{constant}.} \tag{8.11}$$

The current is parallel to the magnetic field, so the Lorentz force vanishes. This is the linear force-free *Taylor state*. The constant α results from imposing one global helicity constraint [9, 10].

The relaxation hypothesis is that extensive reconnection allows the field to approach this minimum while approximately retaining H_m. Strictly ideal evolution preserves much more field-line information and cannot, in general, reach this minimum.

8.5 Finding a relaxed field in a given domain

Taking a curl of equation (8.11), and using $\boldsymbol{\nabla}\cdot\boldsymbol{B}=0$, gives

$$\nabla^2\boldsymbol{B} = -\alpha^2\boldsymbol{B}. \tag{8.12}$$

This helps construct solutions, which must still satisfy the original curl equation and the boundary conditions. For a nonzero α in a simply connected closed magnetic domain, $\boldsymbol{A}=\boldsymbol{B}/\alpha$ is an allowed choice of vector potential. Therefore

$$H_m = \frac{1}{\alpha}\int_V B^2\,\mathrm{d}V, \qquad \boxed{E_B = \frac{\alpha H_m}{2}.} \tag{8.13}$$

The domain determines the allowed branches. At fixed H_m, compare their energies and select the lowest compatible branch; when α is a discrete curl eigenvalue, H_m fixes the field amplitude. Incomplete reconnection or additional surviving constraints can prevent the plasma from reaching this fully relaxed state.

Magnetic helicity constrains how the magnetic field is linked. Cross helicity constrains a different aspect of the state: the correlation between the flow and magnetic field. We turn to that constraint next.

9 Cross helicity and Alfvénic relaxation

9.1 Cross helicity and the energy bound

Continue with the velocity-unit normalization of section 7. For the total fields,

$$\boxed{E = \frac{1}{2}\int_V (U^2 + B^2)\,\mathrm{d}V, \qquad H_c = \int_V \boldsymbol{U}\cdot\boldsymbol{B}\,\mathrm{d}V.} \tag{9.1}$$

Positive cross helicity favours parallel velocity and magnetic field, while negative cross helicity favours antiparallel fields. This is an amplitude-weighted correlation: local regions of opposite sign can cancel in the volume integral.

To find the lowest energy compatible with a given H_c, expand a square:

$$\begin{aligned} E \mp H_c &= \frac{1}{2}\int_V \left(U^2 + B^2 \mp 2\boldsymbol{U}\cdot\boldsymbol{B}\right)\mathrm{d}V \\ &= \frac{1}{2}\int_V |\boldsymbol{U} \mp \boldsymbol{B}|^2\,\mathrm{d}V \geq 0. \end{aligned} \tag{9.2}$$

Both signs together imply

$$\boxed{E \geq |H_c|.} \tag{9.3}$$

If *only* H_c is held fixed, the minimum is attained at $\boldsymbol{U} = \boldsymbol{B}$ for $H_c > 0$, or $\boldsymbol{U} = -\boldsymbol{B}$ for $H_c < 0$. These are Alfvénic states: velocity and magnetic field are aligned or anti-aligned, with equal kinetic and magnetic energy densities at each point. Alignment of directions alone does not attain the bound. If $H_c = 0$, this unconstrained minimum is the zero-field, zero-flow state.

Other constraints, including mean magnetic flux, mean velocity, and magnetic helicity, can prevent this minimum from being attained. For example, a nonzero mean magnetic field and zero mean velocity exclude $\boldsymbol{U} = \pm\boldsymbol{B}$ for the total fields. In section 10, we apply the same bound to fluctuations about a uniform guide field.

9.2 Selective decay toward an Alfvénic state

If dissipation lowers E while $|H_c|$ changes relatively little, the state approaches the energy bound. Such a route toward an Alfvénic state is often called dynamic alignment. Approximate cross-helicity preservation needs a dynamical justification: its dissipative budget does not guarantee it. In ideal MHD, both E and H_c are constant, so conservation alone produces no decay toward the bound.

The limiting state also has a simple dynamical meaning. Substituting $\boldsymbol{U} = \pm\boldsymbol{B}$ into the ideal total-field equations cancels the advective and magnetic-tension terms, and the induction terms cancel as well. Under periodic conditions, the total pressure is spatially constant and the state is stationary.

The combinations $\boldsymbol{U} \pm \boldsymbol{B}$ appearing in the energy bound suggest the Elsasser variables. Their sum and difference will connect cross helicity to the two populations of interacting Alfvénic fluctuations.

10 Elsasser variables, wave packets, and imbalance

10.1 Definitions and inverse relations

Using the velocity-unit normalization introduced in section 7, define the total-field Elsasser variables by

$$\boxed{\boldsymbol{Z}^{\pm} = \boldsymbol{U} \pm \boldsymbol{B}.} \tag{10.1}$$

The inverse relations are

$$\boldsymbol{U} = \frac{\boldsymbol{Z}^+ + \boldsymbol{Z}^-}{2}, \qquad \boldsymbol{B} = \frac{\boldsymbol{Z}^+ - \boldsymbol{Z}^-}{2}. \tag{10.2}$$

This is an exact change of variables in incompressible MHD; all three vector components and all spatial derivatives remain.

10.2 Energy and cross helicity in Elsasser variables

Choose the Elsasser energies to be

$$\boxed{E^\pm = \frac{1}{4}\int_V |\boldsymbol{Z}^\pm|^2 \,\mathrm{d}V.} \tag{10.3}$$

Expanding the square gives

$$E^\pm = \frac{1}{4}\int_V \left(U^2 + B^2 \pm 2\boldsymbol{U}\cdot\boldsymbol{B}\right)\mathrm{d}V = \frac{1}{2}(E \pm H_c). \tag{10.4}$$

Energy is the sum; cross helicity is the difference

$$\boxed{E = E^+ + E^-, \qquad H_c = E^+ - E^-.} \tag{10.5}$$

Since $E^\pm \geq 0$, $E \geq |H_c|$. The minimum at fixed nonzero H_c contains only one Elsasser population.

The kinetic and magnetic energies are

$$E_U = \frac{1}{2}\int_V U^2 \,\mathrm{d}V = \frac{1}{8}\int_V |\boldsymbol{Z}^+ + \boldsymbol{Z}^-|^2 \,\mathrm{d}V, \tag{10.6}$$

$$E_B = \frac{1}{2}\int_V B^2 \,\mathrm{d}V = \frac{1}{8}\int_V |\boldsymbol{Z}^+ - \boldsymbol{Z}^-|^2 \,\mathrm{d}V. \tag{10.7}$$

Their difference, the *residual energy*, is

$$E_U - E_B = \frac{1}{2}\int_V \boldsymbol{Z}^+\cdot\boldsymbol{Z}^- \,\mathrm{d}V. \tag{10.8}$$

Equal Elsasser energies mean zero cross helicity; they do not require kinetic–magnetic equipartition.

10.3 Adding and subtracting the equations

In the same units, the ideal, unforced MHD equations are

$$\partial_t \boldsymbol{U} + (\boldsymbol{U}\cdot\boldsymbol{\nabla})\boldsymbol{U} = -\boldsymbol{\nabla}\Pi + (\boldsymbol{B}\cdot\boldsymbol{\nabla})\boldsymbol{B}, \tag{10.9}$$

$$\partial_t \boldsymbol{B} + (\boldsymbol{U}\cdot\boldsymbol{\nabla})\boldsymbol{B} = (\boldsymbol{B}\cdot\boldsymbol{\nabla})\boldsymbol{U}, \qquad \boldsymbol{\nabla}\cdot\boldsymbol{U} = \boldsymbol{\nabla}\cdot\boldsymbol{B} = 0. \tag{10.10}$$

Here Π is the total pressure per unit mass, with magnetic contribution $B^2/2$. Adding or subtracting the equations combines the nonlinear terms as

$$(\boldsymbol{U}\cdot\boldsymbol{\nabla})\boldsymbol{Z}^\pm \mp (\boldsymbol{B}\cdot\boldsymbol{\nabla})\boldsymbol{Z}^\pm = (\boldsymbol{Z}^\mp\cdot\boldsymbol{\nabla})\boldsymbol{Z}^\pm.$$

Thus

$$\boxed{\partial_t \boldsymbol{Z}^\pm + (\boldsymbol{Z}^\mp\cdot\boldsymbol{\nabla})\boldsymbol{Z}^\pm = -\boldsymbol{\nabla}\Pi, \qquad \boldsymbol{\nabla}\cdot\boldsymbol{Z}^\pm = 0.} \tag{10.11}$$

With periodic boundaries, the two Elsasser energies are separately conserved:

$$\frac{\mathrm{d}E^+}{\mathrm{d}t} = \frac{\mathrm{d}E^-}{\mathrm{d}t} = 0. \tag{10.12}$$

This is equivalent to conservation of E and H_c. The ideal nonlinear terms redistribute each population's energy across scales without changing its volume integral [4].

10.4 Fluctuations about a uniform guide field

Write

$$\boldsymbol{U} = \boldsymbol{U}_0 + \delta\boldsymbol{U}, \qquad \boldsymbol{B} = \boldsymbol{B}_0 + \delta\boldsymbol{B}, \qquad \langle\delta\boldsymbol{U}\rangle = \langle\delta\boldsymbol{B}\rangle = 0. \tag{10.13}$$

Work in the mean-flow frame, $\boldsymbol{U}_0 = 0$, with $\boldsymbol{B}_0 = B_0\boldsymbol{e}_z$ constant. Since the magnetic field is already in velocity units, $v_\mathrm{A} = B_0$. The fluctuating Elsasser fields are

$$\boxed{\delta\boldsymbol{Z}^\pm = \delta\boldsymbol{U} \pm \delta\boldsymbol{B}, \qquad \boldsymbol{Z}^\pm = \pm\boldsymbol{B}_0 + \delta\boldsymbol{Z}^\pm.} \tag{10.14}$$

Define the corresponding fluctuation energies:

$$E_\mathrm{fl}^\pm = \frac{1}{4}\int_V |\delta\boldsymbol{Z}^\pm|^2\,\mathrm{d}V, \tag{10.15}$$

$$E_\mathrm{fl} = \frac{1}{2}\int_V \left(|\delta\boldsymbol{U}|^2 + |\delta\boldsymbol{B}|^2\right)\mathrm{d}V = E_\mathrm{fl}^+ + E_\mathrm{fl}^-, \tag{10.16}$$

$$H_c = \int_V \delta\boldsymbol{U}\cdot\delta\boldsymbol{B}\,\mathrm{d}V = E_\mathrm{fl}^+ - E_\mathrm{fl}^-. \tag{10.17}$$

Total and fluctuation cross helicity agree in this frame. The total energy includes the uniform guide field:

$$E = E_\mathrm{fl} + \frac{VB_0^2}{2}, \qquad E^\pm = E_\mathrm{fl}^\pm + \frac{VB_0^2}{4}. \tag{10.18}$$

The fluctuation energies obey the same algebra and the same ideal conservation laws, since the mean field is constant. The guide-field contribution must be excluded when measuring *turbulent* imbalance.

Substituting the mean–fluctuation split into equation (10.11) gives

$$\partial_t\delta\boldsymbol{Z}^\pm \mp v_\mathrm{A}\partial_z\delta\boldsymbol{Z}^\pm + (\delta\boldsymbol{Z}^\mp\cdot\boldsymbol{\nabla})\delta\boldsymbol{Z}^\pm = -\boldsymbol{\nabla}\Pi, \qquad \boldsymbol{\nabla}\cdot\delta\boldsymbol{Z}^\pm = 0. \tag{10.19}$$

With finite ν and η, the right-hand side additionally contains

$$\frac{\nu+\eta}{2}\nabla^2\delta\boldsymbol{Z}^\pm + \frac{\nu-\eta}{2}\nabla^2\delta\boldsymbol{Z}^\mp. \tag{10.20}$$

Diffusion is diagonal only when $\nu = \eta$.

Our sign convention fixes the propagation direction: the linear + equation is $\partial_t\delta\boldsymbol{Z}^+ - v_\mathrm{A}\partial_z\delta\boldsymbol{Z}^+ = 0$, so its solutions depend on $z + v_\mathrm{A}t$ and travel opposite to the guide field. The − population travels along it. Below, wave packets refer to $\delta\boldsymbol{Z}^\pm$; $\delta Z_\ell^\pm$ denotes a characteristic difference across scale ℓ.

10.5 Why the opposite population matters

There is no term $(\delta\boldsymbol{Z}^+\cdot\boldsymbol{\nabla})\delta\boldsymbol{Z}^+$ in the + equation. The field that advects and strains $\delta\boldsymbol{Z}^+$ is $\delta\boldsymbol{Z}^-$. Consequently, if $\delta\boldsymbol{Z}^- = 0$ everywhere, a solenoidal profile

$$\delta\boldsymbol{Z}^+ = \boldsymbol{F}(x, y, z + v_\mathrm{A}t) \tag{10.21}$$

is an exact solution with spatially constant total pressure. Its shape and amplitude need not be infinitesimal. Several packets in that same population can overlap without generating a nonlinear self-interaction.

When both populations are present, each can distort the other during their overlap. The relative propagation speed is $2v_\mathrm{A}$; for scaling purposes an encounter lasts $\tau_\mathrm{A} \sim \ell_\parallel/v_\mathrm{A}$, with factors of two omitted. Spatial variation across a packet supplies the gradients needed for distortion. Opposite propagation permits an interaction, but special geometries can still make the nonlinear term vanish.

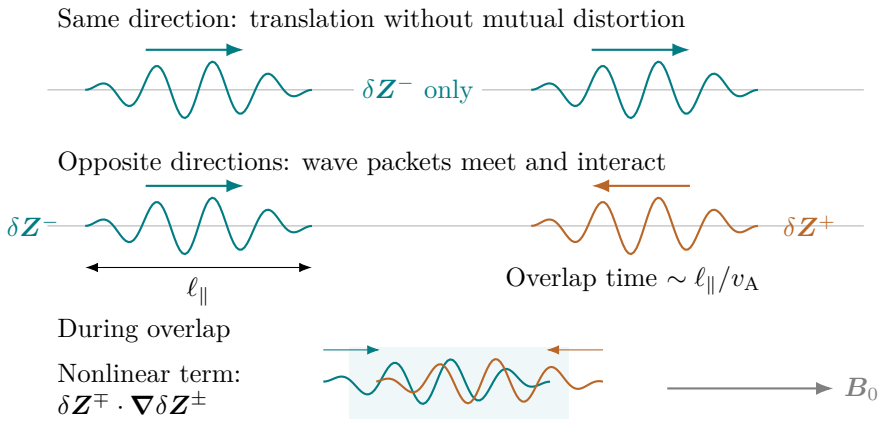


Figure 14: One Elsasser population has no nonlinear self-interaction. Opposite populations can distort one another during overlap. The drawn oscillations are packet profiles, not their perpendicular widths.

Elsasser variables identify the agent of nonlinear distortion

A + packet is strained by the − field, and a − packet by the + field. A uniform advecting field only translates a packet; variation of the opposite field across the packet produces intrinsic distortion. This structure will determine the two nonlinear times and the effect of imbalance.

10.6 Cross helicity measures population imbalance

For nonzero fluctuation energy, define the normalized cross helicity

$$\sigma_c = \frac{H_c}{E_\mathrm{fl}} = \frac{E_\mathrm{fl}^+ - E_\mathrm{fl}^-}{E_\mathrm{fl}^+ + E_\mathrm{fl}^-}, \qquad -1 \le \sigma_c \le 1. \tag{10.22}$$

Balanced turbulence has equal Elsasser energies; the balanced estimates used earlier require comparable amplitudes at the scales being considered. Imbalanced turbulence has unequal populations. A state with $|\sigma_c| = 1$ contains only one population and has $\delta \boldsymbol{U} = \pm \delta \boldsymbol{B}$ everywhere, combining alignment with kinetic–magnetic equipartition. Alignment of directions alone does not ensure this limiting state.

The energy bound now has a direct population interpretation:

$$E_\mathrm{fl} = |H_c| + 2 \min(E_\mathrm{fl}^+, E_\mathrm{fl}^-). \tag{10.23}$$

At fixed fluctuation cross helicity, the minimum energy has no minority population. For $H_c > 0$, $\delta \boldsymbol{Z}^- = 0$ and $\delta \boldsymbol{U} = \delta \boldsymbol{B}$; the opposite sign selects the other population. With a guide field, this is the exactly translating packet in equation (10.21), rather than the stationary total-field state discussed in section 9.

10.7 Imbalance separates the straining times

Let $\delta Z_\ell^\pm$ denote a characteristic increment of $\delta \boldsymbol{Z}^\pm$ across a packet. For perpendicular width $\ell_\perp$ and parallel length $\ell_\parallel$, the usual transverse straining estimates are

$$\tau_\mathrm{nl}^+ \sim \frac{\ell_\perp}{\delta Z_\ell^-}, \qquad \tau_\mathrm{nl}^- \sim \frac{\ell_\perp}{\delta Z_\ell^+}, \qquad \tau_\mathrm{A} \sim \frac{\ell_\parallel}{v_\mathrm{A}}. \tag{10.24}$$

A weak minority population strains the dominant population slowly, while the dominant population can strain the minority rapidly. The corresponding fractional distortion in one encounter is

$$\chi^\pm \sim \frac{\tau_\mathrm{A}}{\tau_\mathrm{nl}^\pm} \sim \frac{\delta Z_\ell^\mp \ell_\parallel}{v_\mathrm{A} \ell_\perp}. \tag{10.25}$$

These estimates identify the strength of an encounter. They do not determine both cascade times in an imbalanced system: the coherence of successive strains and the populations' parallel lengths also matter. The weak and strong cascade arguments in sections 5 and 6 use a balanced baseline, $\delta Z_\ell^+ \sim \delta Z_\ell^-$. They should not be extended to arbitrary imbalance simply by substituting one amplitude [4].

10.8 Global relaxation and local alignment answer different questions

A global $|\sigma_c| \to 1$ means that one population becomes negligible throughout the volume in an energy-weighted sense. Scale-dependent alignment concerns the geometry of local increments. Regions with $\delta\boldsymbol{U} \approx +\delta\boldsymbol{B}$ and regions with $\delta\boldsymbol{U} \approx -\delta\boldsymbol{B}$ can coexist, giving strong local alignment even when the net cross helicity is small.

The global energy bound does not supply a scale-dependent alignment-angle law. We now introduce the additional geometrical assumptions required for that problem.

11 Dynamic alignment and three-dimensional structure

11.1 A finite energy flux needs a finite interaction

The Alfvénic limit explains why alignment can weaken nonlinear evolution. A cascade carrying a nonzero flux must retain departures from that limit. We now ask how local alignment changes the geometry and interaction rate of a strong, globally balanced cascade [7, 8].

Global balance does not prohibit patches with $\delta\boldsymbol{U}$ nearly parallel or antiparallel to $\delta\boldsymbol{B}$: patches of the two signs can cancel in the integrated cross helicity. Conversely, the selective-decay argument for a global energy minimum does not by itself determine a scale-dependent alignment law.

The Elsasser nonlinearity is a directional derivative. A field $\delta\boldsymbol{Z}^-$ strongly distorts $\delta\boldsymbol{Z}^+$ only if it points along a direction in which $\delta\boldsymbol{Z}^+$ varies appreciably. In an aligned structure, the combined polarization and gradient geometry can suppress the interaction. Represent this suppression by a small effective angle θ_λ:

$$\left|\delta\boldsymbol{Z}^\mp \cdot \boldsymbol{\nabla}\delta\boldsymbol{Z}^\pm\right|_\lambda \sim \frac{\delta Z_\lambda^2 \theta_\lambda}{\lambda}, \qquad \boxed{\tau_{\mathrm{nl}} \sim \frac{\lambda}{\delta Z_\lambda \theta_\lambda}.} \tag{11.1}$$

Here δZ_λ is a representative fluctuation amplitude in the ensemble; λ is the shortest perpendicular scale. The angle is a model of the effective nonlinear suppression. It should not simply be identified with the angle between $\delta\boldsymbol{Z}^+$ and $\delta\boldsymbol{Z}^-$. For example, the definition gives $\delta\boldsymbol{Z}^+ \cdot \delta\boldsymbol{Z}^- = |\delta\boldsymbol{U}|^2 - |\delta\boldsymbol{B}|^2$. Where the two local amplitudes are equal in velocity units, this dot product vanishes even when $\delta\boldsymbol{U}$ and $\delta\boldsymbol{B}$ are nearly aligned. The same identity applies to increments across a fixed separation.

11.2 Three lengths instead of two

The structure now has a parallel length $\ell_\parallel$ and two different perpendicular lengths: a thickness λ and a longer coherence length ξ_λ. In the alignment picture,

$$\theta_\lambda \sim \frac{\lambda}{\xi_\lambda}, \qquad \tau_{\mathrm{nl}} \sim \frac{\xi_\lambda}{\delta Z_\lambda}. \tag{11.2}$$

This geometry is consistent with solenoidality: variation of a dominant perpendicular field component over ξ_λ can balance variation of a smaller component across λ. It is a description of an organized structure, not a consequence of $\boldsymbol{\nabla}\cdot\boldsymbol{B} = 0$ alone.

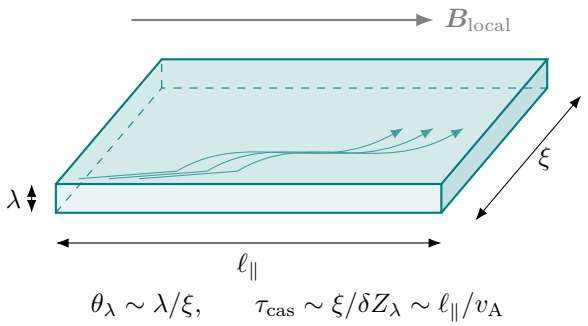


Figure 15: An aligned structure has parallel length $\ell_\parallel$, perpendicular extent ξ, and thickness λ. Dimensions are schematic, not to scale.

Critical balance still compares the propagation time with the *actual* nonlinear time:

$$\frac{\ell_\parallel}{v_{\mathrm{A}}} \sim \frac{\lambda}{\delta Z_\lambda \theta_\lambda}, \qquad \varepsilon \sim \frac{\delta Z_\lambda^3 \theta_\lambda}{\lambda}. \tag{11.3}$$

These two relations do not yet fix a spectral exponent: we also need the scale dependence of θ_λ.

11.3 An alignment closure and its consequences

A classical phenomenological choice is

$$\theta_\lambda \sim \theta_L \left(\frac{\lambda}{L}\right)^{1/4}. \tag{11.4}$$

It expresses increasing alignment toward small scales. Its scale dependence is an additional physical hypothesis, to be tested against geometry and nonlinear-transfer measurements. It does not follow from conservation of cross helicity or from critical balance alone.

With this closure, constant flux gives $\delta Z_\lambda^3 \propto \lambda/\theta_\lambda \propto \lambda^{3/4}$. Therefore,

$$\boxed{\delta Z_\lambda \propto \lambda^{1/4}, \quad E_\perp(k_\perp) \propto k_\perp^{-3/2}, \quad \ell_\parallel \propto \lambda^{1/2}, \quad \xi_\lambda \propto \lambda^{3/4}.} \tag{11.5}$$

Both perpendicular dimensions shrink, but the thickness shrinks faster. The smaller structures become relatively more sheet-like. GS95 and this aligned model both use critical balance; they estimate the nonlinear rate differently.

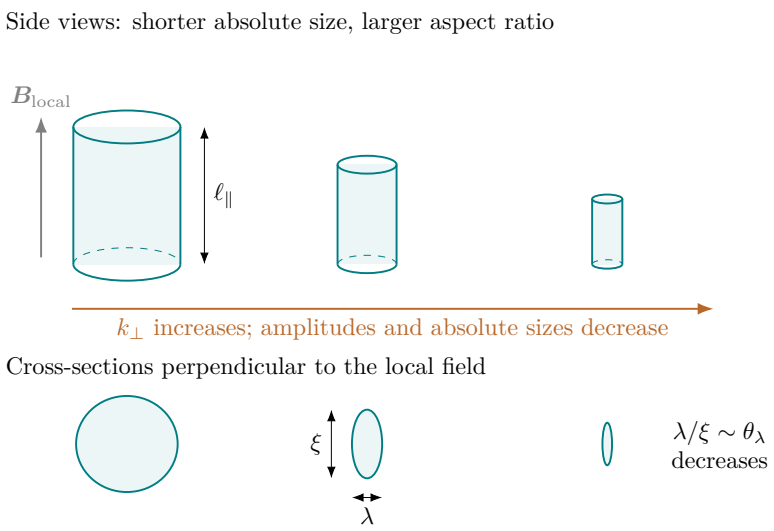


Figure 16: Three-dimensional geometry in the alignment model. Both perpendicular dimensions shrink, while the cross-section becomes relatively more flattened at smaller scales.

One heuristic motivation compares the alignment angle with the uncertainty in the local field direction, of order $\delta B_\lambda/B_0$. If one additionally sets $\theta_\lambda \sim \delta Z_\lambda/v_\mathrm{A}$, the same flux estimate becomes

$$\delta Z_\lambda^4 \sim \varepsilon v_\mathrm{A} \lambda, \qquad E_\perp(k_\perp) \sim (\varepsilon v_\mathrm{A})^{1/2} k_\perp^{-3/2}. \tag{11.6}$$

This is one specific normalization of the model. The equality between the two angles is a closure assumption, rather than a general requirement on fluctuations in a guide field. Keeping θ_L explicit avoids assuming it is fixed by $\delta Z_L/v_\mathrm{A}$ in every system.

If diffusion terminates the aligned cascade, use the modified nonlinear time when comparing with λ^2/η. Under the particular closure $\theta_\lambda \sim \delta Z_\lambda/v_\mathrm{A}$, this gives $\lambda_\eta \sim \eta^{2/3} v_\mathrm{A}^{1/3} \varepsilon^{-1/3}$. Other amplitude normalizations must be carried through consistently.

What alignment adds

The size and amplitude of a fluctuation do not completely determine its nonlinear interaction: directions and internal structure also matter. A spectral slope should therefore be assessed together with anisotropy, alignment, and transfer-time measurements.

12 Intermittency

A spectrum summarizes second-order fluctuations. It does not tell us whether those fluctuations are spread uniformly through the volume or concentrated in rare, intense events. Higher-order moments make that distinction visible:

$$S_q(\ell) = \langle |\delta \boldsymbol{U}_\ell|^q \rangle \propto \ell^{\zeta_q}. \tag{12.1}$$

Here q is the moment order and ζ_q is its scaling exponent. Large q gives greater weight to rare, unusually strong fluctuations.

The self-similar K41 prediction. The amplitude estimate $\delta U_\ell \sim (\varepsilon \ell)^{1/3}$ determines all moment exponents only if we add statistical self-similarity: after division by this amplitude, the *whole distribution* is independent of scale. Write this as

$$\delta \boldsymbol{U}_\ell \overset{\text{distribution}}{=} (\varepsilon \ell)^{1/3} \boldsymbol{X}, \tag{12.2}$$

where the dimensionless random vector $\boldsymbol{X}$ has the same distribution at every inertial-range scale. For an order q with finite $\langle|\boldsymbol{X}|^q\rangle$, taking the absolute moment now takes only one step:

$$S_q(\ell) = (\varepsilon\ell)^{q/3} \underbrace{\langle|\boldsymbol{X}|^q\rangle}_{C_q \text{ independent of } \ell} \quad \Longrightarrow \quad \boxed{\zeta_q = \frac{q}{3}.} \tag{12.3}$$

Thus $\zeta_2 = 2/3$, $\zeta_3 = 1$, and $\zeta_6 = 2$ in this model. More generally, $\zeta_q = (q/p)\zeta_p$: the exponent is proportional to the *moment order*, with slope $1/3$. This is the non-intermittent reference prediction, not an intermittency correction. It also shows why the root-mean-square scaling alone does not determine every higher moment.

What intermittency changes. If the rescaled distribution develops heavier tails at smaller scales, C_q becomes scale dependent. Then high-order moments no longer follow $\zeta_q = q/3$; the curve of ζ_q versus q bends. A simple diagnostic is that $S_q/S_2^{q/2}$ is constant for perfect self-similarity but varies with scale in intermittent turbulence. The same test can be applied to magnetic or Elsasser increments, using the reference scaling of the model being tested.

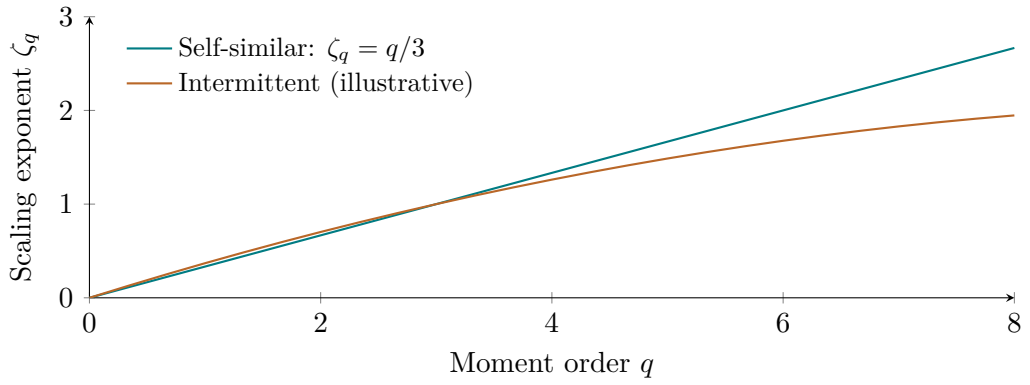


Figure 17: Simple self-similarity gives a linear dependence of the moment exponent on its order; intermittency can bend this relation. The curved line is illustrative.

References

[1] U. Frisch (1995), *Turbulence: The Legacy of A. N. Kolmogorov*. Cambridge University Press. 10.1017/CBO9781139170666.

[2] G. K. Batchelor (1953), *The Theory of Homogeneous Turbulence*. Cambridge University Press.

[3] D. Biskamp (2003), *Magnetohydrodynamic Turbulence*. Cambridge University Press. 10.1017/CBO9780511535222.

[4] A. A. Schekochihin (2022), "MHD turbulence: a biased review," *Journal of Plasma Physics* **88**, 155880501. 10.1017/S0022377822000721.

[5] P. Goldreich and S. Sridhar (1995), "Toward a theory of interstellar turbulence. II. Strong Alfvénic turbulence," *The Astrophysical Journal* **438**, 763–775. 10.1086/175121.

[6] S. Galtier, S. V. Nazarenko, A. C. Newell, and A. Pouquet (2000), "A weak turbulence theory for incompressible magnetohydrodynamics," *Journal of Plasma Physics* **63**, 447–488. 10.1017/S0022377899008284.

[7] S. Boldyrev (2006), "Spectrum of magnetohydrodynamic turbulence," *Physical Review Letters* **96**, 115002. 10.1103/PhysRevLett.96.115002.

[8] J. Mason, F. Cattaneo, and S. Boldyrev (2006), "Dynamic alignment in driven magnetohydrodynamic turbulence," *Physical Review Letters* **97**, 255002. 10.1103/PhysRevLett.97.255002.

[9] L. Woltjer (1958), "A theorem on force-free magnetic fields," *Proceedings of the National Academy of Sciences* **44**, 489–491. 10.1073/pnas.44.6.489.

[10] J. B. Taylor (1986), "Relaxation and magnetic reconnection in plasmas," *Reviews of Modern Physics* **58**, 741–763. 10.1103/RevModPhys.58.741.